

THIS IS THE UNEDITED, UNCORRECTED AUTHORS' VERSION OF AN ARTICLE ACCEPTED FOR PUBLICATION IN the Elsevier journal *Neuroimage*. PLEASE CITE THIS WORK AS FOLLOWS: Vallesi A., Del Felice A., Capizzi M., Tafuro A., Formaggio E., Bisiacchi P., Masiero S., Ambrosini E. (in press). Natural oscillation frequencies in the two lateral prefrontal cortices induced by Transcranial Magnetic Stimulation. *Neuroimage*. DOI: 10.1016/j.neuroimage.2020.117655.

Running head: Prefrontal natural frequencies

Natural oscillation frequencies in the two lateral prefrontal cortices induced by Transcranial Magnetic Stimulation

Antonino Vallesi^{1,2,#}, Alessandra Del Felice¹, Mariagrazia Capizzi³, Alessandra Tafuro⁴, Emanuela Formaggio⁴, Patrizia Bisiacchi⁵, Stefano Masiero¹, Ettore Ambrosini^{1,5,#}

¹ Department of Neuroscience & Padova Neuroscience Center, University of Padua, Padua, Italy

² Brain Imaging and Neural Dynamics Research Group, IRCCS, San Camillo Hospital, Venice Italy

³ EA 4556 EPSYLON, Université Paul Valéry, Montpellier 3, France

⁴ Department of Neuroscience, University of Padua, Padua, Italy

⁵ Department of General Psychology, University of Padua, Padua, Italy

Correspondence should be sent to:

Ettore Ambrosini, Department of Neuroscience & Padova Neuroscience Center, University of Padua, 35131 Padua, Italy. E-mail: ettore.ambrosini@unipd.it

Antonino Vallesi, Department of Neuroscience & Padova Neuroscience Center, University of Padua, 35131 Padua, Italy. E-mail: antonino.vallesi@unipd.it

Abstract

Different cortical regions respond with distinct rhythmic patterns of neural oscillations to Transcranial Magnetic Stimulation (TMS). We investigated natural frequencies induced by TMS in left and right homologous dorsolateral prefrontal cortices (DLPFC) and related hemispheric differences. In 12 healthy young adults, single-pulse TMS was delivered in different blocks close to F3 and F4 channels to target left and right DLPFC. An occipital site near PO3 was stimulated as control. TMS-related spectral perturbation analyses were performed on recorded EEG data. A widespread unspecific increase in theta power was observed for all stimulation sites. However, occipital TMS induced greater alpha activity and a 10.58 Hz natural frequency, while TMS over the left and right DLPFC resulted in similar beta band modulations and a natural frequency of 18.77 and 18.5 Hz, respectively. More specifically, TMS-related specific increase in beta activity was stronger for the right than the left DLPFC. The right DLPFC is more specifically tuned to its natural beta frequency when it is directly stimulated by TMS than with TMS over the left counterpart (or a posterior region), while the left DLPFC increases its beta activity more similarly irrespective of whether it is directly stimulated or through right homologous stimulation. These results yield important implications for both basic neuroscience research on inter-hemispheric prefrontal interactions and clinical applications.

Keywords: Natural Brain Oscillations; Event-related Spectral Perturbation; Single-Pulse Transcranial Magnetic Stimulation; TMS-EEG co-registration; dorsolateral prefrontal cortex

1. Introduction

Rhythmic patterns of neural oscillations are believed to play a functional role in local processing and communication between different neuronal systems (Fries, 2005; Thut et al., 2012). Different human cortical regions tend to oscillate at distinct frequencies. For instance, a strong association has been documented between electroencephalography (EEG) alpha desynchronization and occipital Blood-Oxygen-Level-Dependent (BOLD)-activity (Feige et al., 2005; Laufs et al., 2003; Moosmann et al., 2003), whereas activity of the dorsal attention fronto-parietal network is associated with higher (alpha and beta) rhythms than visual network activity (Mantini et al., 2007).

However, correlating highly unstable resting-state EEG activity with BOLD-response is not a definitive method to draw causal inferences about the frequency tuning of cortical areas. A more reliable approach consists of coupling neurostimulation techniques with simultaneous EEG-recording to detect whether stimulated cortical areas are tuned to oscillate at a preferred rate, the so-called natural frequency (Rosanova et al., 2009; Thut et al., 2011). In the seminal work by Rosanova and colleagues (2009), single-pulse Transcranial Magnetic Stimulation (sp-TMS) produced global changes in spectral power, so-called Event-Related Spectral Perturbations (ERSP), characterized by dominant alpha oscillations (8-12 Hz) when applied over the left associative occipital cortex (Brodmann area, BA, 19), low beta oscillations (13-20 Hz) over the left superior parietal lobule (BA 7), and faster frequencies (21-50 Hz) over the left premotor cortex (BA 6) (in-silico simulation in Cona et al., 2011). Vigilance state also modulates evoked activity by resonating in the EEG rhythm proper of the state (Manganotti et al., 2013). These oscillations have been suggested to reflect local, intrinsic physiological mechanisms related to the fine-tuning of corticothalamic circuits: each cortical region tended to resonate at approximately the same frequency not only when TMS was directly applied, but also when it was applied to two other hot-spots, possibly because of the cortico-cortical spreading of the TMS-induced electrical activity (Rosanova et al., 2009).

The study of natural frequencies does not only have theoretical relevance but also clinical implications. For instance, individuals with schizophrenia show a natural frequency reduction that follows a caudo-rostral gradient when compared to healthy controls (Ferrarelli et al., 2012), with a progressively more pronounced frequency slowing towards the prefrontal cortex. A reduction of dominant frequencies of premotor EEG responses to TMS also characterizes bipolar disorder and major depression (Canali et al., 2017, 2015).

As mentioned above, only a previous study (Ferrarelli et al., 2012) investigated the TMS-induced natural frequency of a prefrontal region located more anteriorly than the premotor cortex, namely the left middle frontal gyrus close to the midline, and found that this region responded with a wide range of frequencies spanning from high beta to gamma, with a natural frequency centered at 31 Hz in healthy individuals.

Overall, these two previous studies (Ferrarelli et al., 2012; Rosanova et al., 2009) reported a hierarchical gradient directed from slower frequencies caudally to faster frequencies towards the prefrontal cortex. However, another study (preprint in Stanfield and Wiener, 2019), which used the same approach to target three scalp regions over the right hemisphere (P4, C4, F4), instead of the previously probed left hemisphere (Ferrarelli et al., 2012; Rosanova et al., 2009), highlighted a high inter-subject variability and failed to show this rostro-caudal gradient. A similar absence of a gradient was also reported in a resting-state electrocorticographic study (Groppe et al., 2013).

While previous TMS-EEG investigations of natural frequencies focused either on the left (Ferrarelli et al., 2012; Rosanova et al., 2009) or the right (Stanfield and Wiener, 2019) hemisphere separately, no previous work has compared homologous regions in both hemispheres within the same individuals. Therefore, in the present study we targeted the two homologous dorsolateral prefrontal cortices (DLPFC) to investigate hemispheric lateralization of natural frequency distributions. This rationale was based on evidence showing that these two prefrontal regions are functionally dissociable (e.g., Ambrosini and Vallesi, 2016; Habib et al., 2003; Stuss and

Alexander, 2007; Vallesi, 2012). To document the natural frequencies of DLPFC may be critical to guide future neurostimulation applications, given its hierarchically superior role in prefrontal cortical organization (Nee and D'Esposito, 2017).

In particular, we decided to focus our analyses on two channels of the EEG 10/20 system, namely F3 and F4, which are chosen very often as the target for TMS studies, both in basic neuroscience research and clinical interventions (Beam et al., 2009; Finisguerra et al., 2019; Fitzgerald and Daskalakis, 2012; Herwig et al., 2003; Hone-Blanchet et al., 2015), and which are widely used as scalp proxies to target the underlying left and right DLPFC when neuronavigation is unavailable (Fitzgerald et al., 2009; Fox et al., 2013). The PO3 channel, approximately corresponding to the dorsal occipital cortex (DOC), was additionally chosen for comparison with previous TMS-EEG investigations of natural frequencies (Ferrarelli et al., 2012; Rosanova et al., 2009). Indeed, albeit our aim was not to simply replicate these studies, we sought to verify whether our method was effective in evoking the ERSP characterized by the previously reported dominant alpha oscillations in the DOC.

Based on previous resting-state electrocorticogram (Groppe et al., 2013) and TMS-EEG (Ferrarelli et al., 2012) studies, we hypothesized that TMS on the two DLPFCs would evoke ERSP with natural frequencies centered around the beta or beta/gamma range. Of note, left-right lateralization of resting-state beta activity (12.5-24 Hz) in mid-DLPFC, when divided by alpha (β/α index), has been shown to be behaviourally relevant, as it predicted performance in a wide range of executive function tasks (Ambrosini et al., 2020; Ambrosini and Vallesi, 2017, 2016). Instead, we expected a natural frequency around the alpha band in the posterior PO3 site (Ferrarelli et al., 2012; Rosanova et al., 2009).

Of note, none of the previous works (Ferrarelli et al., 2012; Rosanova et al., 2009; Stanfield and Wiener, 2019) directly compared TMS-related ERSP across stimulation sites with a formal statistical test. However, this is important to isolate ERSP modulations specifically caused by TMS

over the target site from unspecific TMS effects like volume conduction (Rosanova et al., 2009) or the cortico-cortical spreading of the TMS-induced activity (Bortoletto et al., 2015). We thus performed a cross-site statistical comparison to understand how specific each TMS-related spectral response was for each stimulation site and to identify the natural frequency of these responses.

2. Materials and methods

2.1 Participants

Twelve healthy young participants (6 females, mean age = 23.4 years, SD = 3.1 years, range = 21-30 years), all native Italian speakers, were recruited after signing an informed consent. A sensitivity power analysis conducted on G*Power (Faul et al., 2009) revealed that our sample size was large enough to have a statistical power ($1-\beta$) of .80 to detect within-subjects significant differences ($\alpha = .05$) corresponding to an effect size (Cohen's d) of .6 assuming a correlation between repeated measures of .75, both conservatively estimated based on a pilot study¹. The effect size was estimated to be conservatively lower than that estimated from the data reported in the existing studies investigating natural frequencies (Ferrarelli et al., 2012; Rosanova et al., 2009)

Participants had normal or corrected-to-normal vision and reported no history of neuropsychiatric illness or epilepsy, and had no contraindication to TMS (Rossi et al., 2009). The Edinburgh Handedness Inventory (EHI, Oldfield, 1971) was used to measure participants' handedness (average EHI score = 52.9, SD = 6.1, range = -65-100). The sample comprised three left-handed participants (EHI scores < -55) and one ambidextrous participant (EHI score = 5), but the results were substantially unvaried when they were excluded (see Supplementary Material). The experimental research received ethical approval from the local Research Ethics Committee at the

¹ As a part of an unpublished study, we used neuro-navigated TMS-EEG to stimulate left and right DLPFC. Pilot results ($n = 4$) revealed that these regions showed specific TMS-dependent spectral activity with large effect sizes ($d > 1$).

University of Padova and was conducted according to the guidelines of the World Medical Association Declaration of Helsinki.

2.2 TMS

The DuoMAG XT-100 bi-phasic transcranial magnetic stimulator (Deymed, Payette, ID) was used for magnetic stimulation with a 70-mm air-cooled figure-of-eight coil. We selected three putative cortical sites to be stimulated: the left and right DLPFC (lDLPFC and rDLPFC, respectively) and the left DOC. The DLPFC scalp sites (approximately corresponding to the mid-posterior middle frontal gyrus) were chosen to verify our hypothesis of an involvement of frequencies in the beta/gamma range in the DLPFC intrinsic spectral activity. The site to stimulate the DLPFC of the motor dominant hemisphere was localized 5 cm rostrally to the scalp motor hot-spot, which in turn was localized by identifying the resting motor threshold (rMT, see below). The symmetric scalp site on the opposite hemisphere was used to stimulate the homologous DLPFC. The scalp stimulation sites for the lDLPFC and rDLPFC were roughly in between F3-FFC3h and F4-FFC4h electrodes, respectively. As a control site, the DOC was targeted by applying TMS over the scalp location corresponding to the midpoint between the POz and PO3 to match the position stimulated in (Rosanova et al., 2009), while avoiding TMS directly over PO3. The stimulation sites were localized over the scalp individually and were marked on the EEG cap worn by participants. The coil was placed tangentially to the scalp with the handle pointing downwards. A mechanical arm was used to ensure the coil was maintained in the same position throughout the whole duration of the experiment.

TMS intensity was set as 100% of individual rMT, which was determined at the beginning of the experiment using a standard procedure (Rossini et al., 1994). The scalp motor hot-spot was localized as the point where a sp-TMS elicited the maximum motor-evoked potential (MEP) from the relaxed abductor pollicis brevis muscle of the dominant hand. MEPs were registered by surface

electrodes using the electromyographic (EMG) system integrated in the DuoMAG. The amplified and bandpass-filtered (50 Hz to 5 kHz) signal was acquired at a sampling rate of 5 kHz; rastered traces recorded evoked potentials (10 ms sweep, 50 μ V). After the motor hotspot was identified, the coil was maintained in the same position, and the rMT was determined as the lowest TMS intensity which produced at least 5 MEPs $\geq 50 \mu$ V out of 10 consecutive stimuli (Rossini et al., 1994). The mean rMT was 52.9% of the maximum stimulator output intensity (SD = 6.1%, range = 44-62%).

We additionally estimated the electrical field intensity induced by TMS on the cortical surface by performing electrical field modelling using the SimNIBS software (Thielscher et al., 2015) on a standardized MNI template. Each cortical area was stimulated, on average, at 79.7 V/m (SD = 9.1 V/m, range = 61.3-93.6 V/m), well above the intensity previously reported as minimal for evoking dominant frequencies (Rosanova et al., 2009). We decided to stimulate at the rMT only, rather than parametrically manipulating the stimulation intensity, as it has already been shown that “the specific frequency of the response did not depend on stimulation intensity, or activation threshold” (Rosanova et al., 2009, p. 7683), at least for intensities >40 V/m, although higher stimulation intensities evoked progressively larger responses in all frequency bands (Rosanova et al., 2009).

Next, three sp-TMS blocks were performed, one for each stimulation site (DOC, IDLPFC, and rDLPFC), in the same day, with a brief break between them (M = 3.9 min, SD = 2.6 min). The order of the blocks was counterbalanced across participants. For each stimulation site, between 150 and 160 TMS single pulses were delivered at a frequency jittering between .4 and .5 Hz (i.e., inter-pulse interval between 2000 and 2500 ms). All stimulation parameters were set according to international safety guidelines (Rossi et al., 2009; Wassermann, 1998).

2.3 EEG recording and preprocessing

The EEG data were recorded (sampling rate = 5000 Hz; online filter = 0.1-1000 Hz) using MR-compatible BrainAmp amplifiers (Brain Products, Germany) from 64 Ag/AgCl electrodes

mounted on a TMS-compatible elastic cap (EASYCAP GmbH, Germany). Impedance was $\leq 6 \text{ k}\Omega$ (grand mean = $3.13 \text{ k}\Omega$, SD = $1.20 \text{ k}\Omega$). All electrodes were referenced to FCz during the recording, while AFz was used as ground. To minimize contamination of TMS-evoked potentials by auditory potentials evoked by the click associated with the TMS discharge and to increase comfort, participants wore inserted earplugs during the whole TMS blocks.

The analysis of participants' EEG data from each recording block was performed with MATLAB v. 2017b (The MathWorks, Natick, MA) using scripts and functions from EEGLAB (v. 13.4.4b; Delorme & Makeig, 2004) and the TESA plugin for EEGLAB (Rogasch et al., 2017). The temporal alignment of EEG data to TMS pulses was controlled and corrected and the EEG data were epoched from -1450 to 1450 ms around the TMS pulse. Such a large time window was chosen to allow extracting the baseline for later wavelet transform² (see section 2.4) while avoiding contamination by TMS-dependent activity from both the previous and current trial (see Figure S1 in Supplementary Material). Next, EEG data were DC-corrected and the TMS pulse artifact and the peak of TMS-evoked muscle activity (see Figure S2 in Supplementary Material, see also Figure 1 in Rogasch et al., 2014; 2017) were removed (from -2 to 18 ms) and replaced with constant amplitude data to improve ICA performance (Rogasch et al., 2017). A visual inspection revealed the absence of disconnected electrodes or trials with large, non-repeating artifacts (e.g., from jaw clenching or head scratching) that could have considerably worsened ICA decomposition, so no manual channel/epoch rejection was performed at this stage.

At this point, residual TMS-evoked muscle and electrical/movement artifacts are still present in the data, as these artifacts last longer than the first 18 ms we removed (see Figure S3 in Supplementary Material). Therefore, as suggested by Rogasch et al. (2018), a first ICA was performed using the FastICA algorithm to remove independent components (ICs) reflecting these

² Indeed, in order to estimate time-frequency information between -1000 and 1000 ms, using 3 cycles for 4 Hz, epochs should be at least 420 ms larger on both sides, as the EEGLAB *newtimef* function generates windows of approximately 840 ms.

large residual TMS-evoked artifacts (Rogasch et al., 2017) via manual selection (see Figures S3-S4 in Supplementary Material). Indeed, these artifacts can affect the accuracy of ICA when used for recovering neural activity or removing physiological artifacts. Moreover, removing these artifacts allows for filtering (without introducing further artifacts, see Figures S4-S5 in Supplementary Material), which may further improve ICA decomposition. The ICA was performed on a temporary dataset re-epoched from -1000 to 1000 ms around the TMS pulse to avoid data overlap, which can bias ICA performance, and the ICA solution was then applied to the original dataset. On average, 2.33 ICs (SD = 0.80, range = 1-3) were removed at this stage, ensuring that EEG data for all participants and TMS blocks were no more contaminated by TMS-evoked muscular artifacts.

Next, constant amplitude data around TMS pulse were linearly interpolated and EEG data were down-sampled at 500 Hz and filtered using zero-phase Blackman-windowed FIR filters (cut-off frequencies = 2 and 45 Hz, transition bandwidth = 2 and 10 Hz) to eliminate line noise and improve subsequent preprocessing steps (see Figure S5 in Supplementary Material). Bad channels were then detected and removed using the *clean_channels* function (correlation threshold = .7; 0.5 channels were excluded on average, SD = .7, range = 0-2) and a second ICA was performed, followed by equivalent dipole fitting, to remove residual TMS artifacts and artifacts due to eye movements, blinks, and muscular activity based on IC scalp maps (see Figure S6 in Supplementary Material), dipole location, power spectrum, and time course. Again, the ICA was performed on a temporary dataset free of data overlap. On average, 22.56 ICs (SD = 3.98, range = 14-29) were removed at this stage. The quality of our ICA decomposition is indicated by the high number of the neural ICs extracted, that is, those with a clear dipolar scalp distribution (Delorme et al., 2012; see Figure S6 in Supplementary Material) and at least 85% of their scalp map variance explained by the best-fitting single equivalent dipole model (Artoni, Delorme & Makeig, 2018). This suggests that our preprocessing was effective in minimizing TMS-related and other artifacts, while retaining the neural signal of interest.

Then, bad channels were interpolated by using a spherical spline method (Perrin et al., 1989), data were re-referenced to a common average reference, and an automatic procedure was used to detect artifactual epochs based on extreme values ($\pm 125 \mu\text{V}$), abnormal trend in data (slope = $100 \mu\text{V}/\text{epoch}$, $R^2 = .3$), and improbability and kurtosis criteria ($\text{SD} > 6$ for single-channel and $\text{SD} > 4$ for global threshold). This procedure was used in addition to the TrialByTrial plugin of EEGLAB: if an epoch had six or more bad channels, it was removed; otherwise, the bad channels were interpolated. This approach allows retaining the maximum number of available epochs (thus improving the reliability of the results) while still maximizing artifact rejection within individual epochs and it is similar to those implemented in various automated EEG preprocessing pipelines, especially for high-artifact data (e.g., FASTER, Nolan, Whelan, & Reilly, 2010; HAPPE, Gabard-Durnam, Mendez Leal, Wilkinson, & Levin, 2018). The average number of retained epochs was 147.8, 148.8, and 147.8, respectively, for the DOC, IDLPFC, and rDLPFC TMS blocks (range = 142-152, 146-160, and 144-153, respectively).

Before performing the ERSP analyses, we analysed the auditory-evoked potentials (AEP) related to the TMS noise, as the use of earplugs (instead of active noise masking) may have masked it only partially³. To this aim, for each participant and TMS block, we extracted the N1 and the P2 components (Conde et al., 2019) by averaging the TMS-evoked potentials (TEPs) recorded over FCz and the eight surrounding electrodes (F1, Fz, F2, FC1, FC2, C1, Cz, and C2) in the time windows from 70 to 130 ms and from 160 to 220 ms, respectively (see Figure S8 in Supplementary Material). The choice of the channels and time windows was based on a multivariate analysis performed on all the TEPs at the single-trial level to blindly identify the peaks of the AEP response. Both N1 and P2 components of the AEP were evident over frontocentral channels, albeit small in

³ Note however that the AEPs that might have been evoked by the TMS click were assumed to be similar for the three TMS sites (because the auditory stimulation can be assumed to be virtually the same across the TMS sites) and, thus, they were controlled for by our analytical approach (see sections 2.4 and 4)

amplitude. Crucially, they did not vary significantly across stimulation sites (N1: $F(2,22) = 0.90$, $p = .422$; P2: $F(2,22) = 2.10$, $p = .146$), confirming our assumption (see footnote 2).

2.4 Scalp-based Event-Related Spectral Perturbation (ERSP) analysis

Time-frequency decomposition was performed via modified complex Morlet wavelet convolution as implemented in the EEGLAB *newtimef* function. To track the significant TMS-related spectral modulations during the post-TMS period, we extracted ERSP between 4 and 45 Hz (frequency resolution = .25 Hz; temporal resolution = 10 ms) at the single trial level using a number of cycles that linearly increased from 3 at the lowest frequency up to 20 at the highest frequency. By using an increasing number of cycles, this method provides a better frequency resolution at higher frequencies as compared to a conventional wavelet approach, which uses a fixed number of cycles (Delorme & Makeig, 2004). ERSPs were expressed in decibel relative to the mean power in the baseline interval from -1000 to -500 ms (single-trial divisive normalization, Grandchamp and Delorme, 2011). This baseline was chosen to be as large as possible while avoiding contaminations by TMS-evoked activity (in both the current and previous trial) due to the temporal smearing resulting from the wavelet transform (see Footnote 1; see also Figures S1 and S7 in Supplementary Material).

Significant ERSPs were detected using the Threshold Free Cluster Enhancement (TFCE) approach, which has the advantage of avoiding a-priori assumptions about data while correcting for multiple comparisons (Smith and Nichols, 2009). One-tailed t-tests were computed over the 165 frequencies ranging from 4 to 45 Hz and the 201 timepoints ranging from -1000 to 1000 ms (to exclude edge artifacts resulting from the wavelet transform and across-trials overlapping of the TMS-related activity). Statistical significance was set at $p = .05$ (2000 permutations).

We first assessed whether TMS modulated the spectral activity of the stimulated cortical regions. For each TMS block, we tested for significant ERSPs on the target channel (i.e., the one

closest to the scalp stimulation sites: PO3, F3, and F4 for the DOC, IDLPFC, and rDLPFC block, respectively). We then tested for the spectral specificity of the TMS effects on ERSPs. For each channel of interest, we compared the ERSP across the three TMS blocks using TFCE. In this way, we detected the ERSPs specifically caused by the TMS over the target channel, rather than by unspecific effects of the TMS or volume conduction.

Next, we assessed the natural frequency of each stimulated cortical site, that is, the main frequency of the local TMS-related oscillations. For each TMS site and participant, we first averaged the ERSP values for the target channel between 20 and 400 ms and compared these power spectrum profiles across TMS sites with paired-sample t-tests corrected for across-frequencies multiple comparisons with the TFCE approach. This temporal window was chosen so to minimize the impact of stereotypical, broadband ERSP modulations occurring around the TMS pulse (Ferrarelli et al., 2012), while capturing the entirety of the TMS-dependent ERSP modulations in our data (Figure 2). Subsequently, for each TMS site, we computed individual natural frequencies from individual power spectrum profiles as the frequency with the maximum value within the frequency band showing a significant, specific TMS-dependent modulation.

2.5 Source-based Event-Related Spectral Perturbation (ERSP) analysis

Source-reconstructed time series of TMS-related EEG activity were obtained by using Brainstorm toolbox (Tadel et al., 2011). We estimated the current strength dynamics of the EEG cortical sources using the depth-weighted minimum norm estimation approach (Baillet et al., 2000) and a boundary element methods conductive head model generated with OpenMEEG (Gramfort, Papadopoulo, Olivi & Clerc, 2010) using the adaptive integration method. The solution space was constrained to the cerebral cortex, which was modelled as a three-dimensional grid of 15002 vertices representing elementary current dipoles with unconstrained orientations based on the FreeSurfer brain template (Fischl, Sereno, Tootell & Dale, 1999).

Three regions of interest (ROI) corresponding to the three intended cortical TMS sites were selected based on the Destrieux atlas (Destrieux, Fischl, Dale & Halgren, 2010) as the left superior occipital gyrus (DOC) and the posterior part of the left (IDLPFC) and right (rDLPFC) middle frontal gyri (see Figure 1A). The DOC ROI (in green in Figure 1A) corresponds to the left superior occipital gyrus, which consisted in 76 vertices (8.26 cm²). The IDLPFC and rDLPFC ROIs (in light purple in Figure 1A) correspond to the posterior part of the left and right middle frontal gyri, respectively. They were created so that their spatial extent (respectively, 69 and 71 vertices, 7.93 and 7.85 cm²) was as similar as possible to the DOC site. The activity for each of these ROIs was estimated by taking the first component from a principal component analysis performed on the current strength time course of each dipole within each ROI. Time-frequency decomposition and statistical analyses of source-based ERSPs were performed as detailed above (see section 2.4).

To support the choice of these ROIs, we examined the cortical distribution of the activity elicited by the TMS. To this aim, the current strength time courses were first normalized (absolute z-transformation) relative to the same baseline interval used for the ERSP analysis (from -1000 to -500 ms) and then averaged over the first 400 ms after TMS (note that the results are substantially the same when using different time windows). As shown in Figure 1B, TMS mainly elicited cortical activity over the target brain regions, suggesting that we successfully targeted the intended cortical regions (but see Discussion for the limitations of our approach).

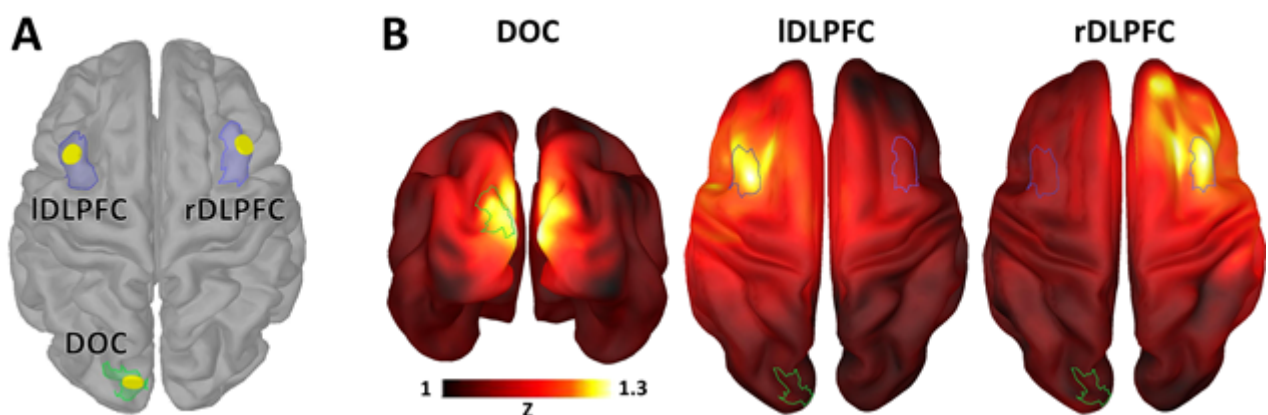


Figure 1. Cortical TMS sites. Panel **A** shows the approximate estimated location of the three cortical sites targeted by TMS (in yellow). They were localized on the FreeSurfer brain template (FSAverage, available in Brainstorm) by projecting the TMS scalp sites onto the cortical surface. The corresponding cortical regions of interest (ROIs) used in the analyses are also shown. Panel **B** shows the average cortical activity elicited during the first 400 ms after TMS for each stimulation site (DOC, dorsal occipital cortex; IDLPFC, left dorsolateral prefrontal cortex; rDLPFC, right dorsolateral prefrontal cortex). See section 2.5 for details.

3. Results

3.1 Event-Related Spectral Perturbations (ERSP)

Figure 2 shows the mean ERSPs after TMS of each site (DOC, IDLPFC, and rDLPFC) for the target channels (PO3, F3, and F4). TMS elicited several EEG oscillations in different frequency bands, with an unspecific increase in theta power that was evident for all stimulation sites and target channels. However, the magnitude and the frequency content of the ERSP responses to TMS also varied markedly as a function of the stimulated site and recorded channels. Indeed, not only the TMS-related increase in power was larger for the target closest to the stimulation site (depicted in the three time-frequency plots labelled as “TMS”), but it also involved higher frequencies for the TMS over prefrontal sites as opposed to the TMS over the occipital site.

Figure 3 shows the scalp distribution of the average ERSP modulations in the theta (4-8 Hz), alpha (8-12 Hz), and beta2 (18-24 Hz) frequency bands during the first 400 ms after TMS (note that the results are substantially the same when using different time windows), indicating that the TMS-dependent ERSP modulations were stronger near the stimulation site, especially for alpha and beta2 bands.

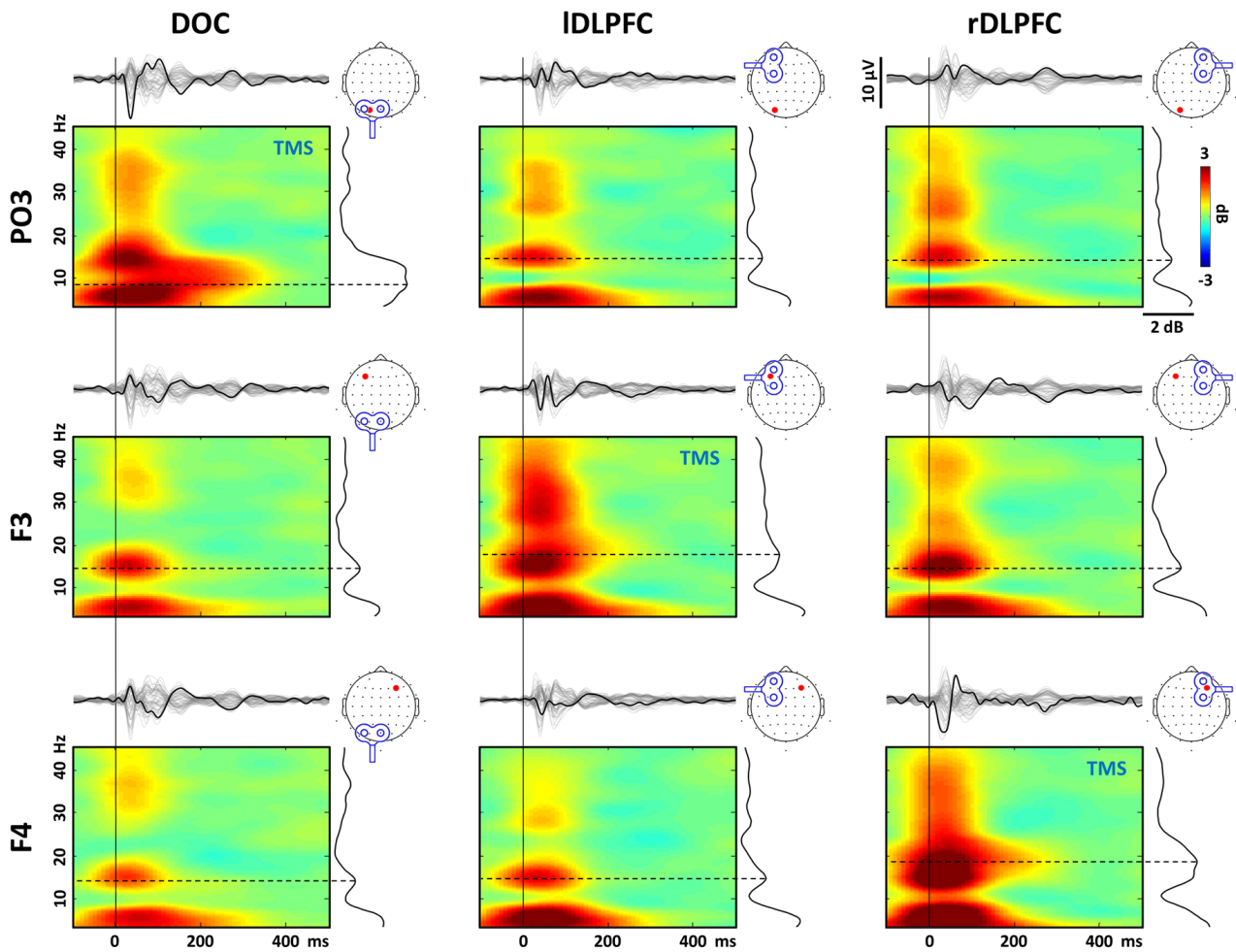


Figure 2. Average scalp-based Event-Related Spectral Perturbations (ERSP). The time-frequency plots show the average TMS-related ERSPs recorded from three different channels (PO3, F3, F4) as a function of the three different stimulation sites (DOC, IDLPFC, rDLPFC). The time-frequency plots on the diagonal line marked by the TMS label show the ERSP for the channel closest to the TMS site. The trace plots above each time-frequency plot represent butterfly plots of all channels, where the black trace highlights the channel directly underlying the stimulator. The black line plotted at the right of each time-frequency plot depicts the power spectrum profile elicited during the first 400 ms after TMS. The black dashed lines highlight the frequency corresponding to the natural frequency.

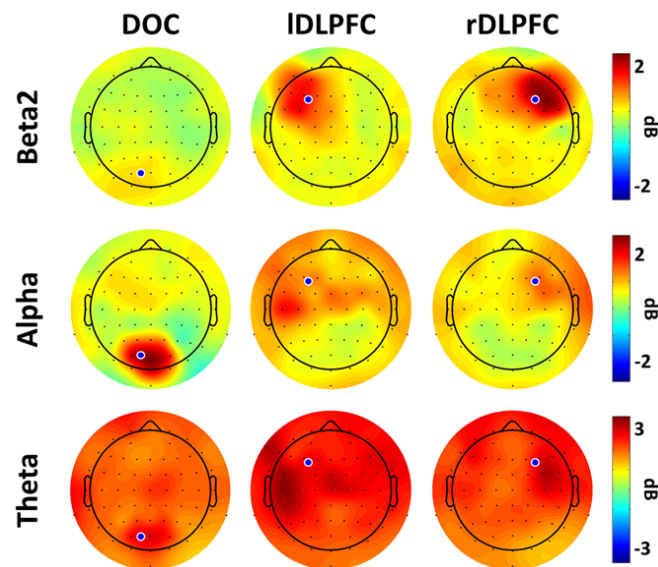


Figure 3. Scalp distribution of the ERSP modulations. The topoplots show the scalp distribution of the average ERSP modulations in the theta (4-8 Hz, bottom row), alpha (8-12 Hz, middle row), and beta2 (18-24 Hz, top row) frequency bands during the first 400 ms after TMS in the three TMS blocks (DOC, dorsal occipital cortex; IDLPFC, left dorsolateral prefrontal cortex; rDLPFC, right dorsolateral prefrontal cortex). The blue dot indicates the TMS scalp site.

Source-based ERSPs were generally consistent with those observed at the scalp level. Figure 4 shows the mean ERSPs after each TMS block (DOC, IDLPFC, and rDLPFC, in columns) for each corresponding ROI (in rows). TMS elicited several EEG oscillations in different frequency bands, with an unspecific increase in theta and alpha power that was evident for all TMS sites and blocks. However, the magnitude and the frequency content of the ERSP responses to TMS also varied markedly as a function of the TMS site and block. Indeed, not only the TMS-related increase in power was larger for the target site (depicted in the three time-frequency plots labelled as “TMS”), but it also involved higher frequencies for the TMS over prefrontal sites as opposed to the TMS over the occipital site.

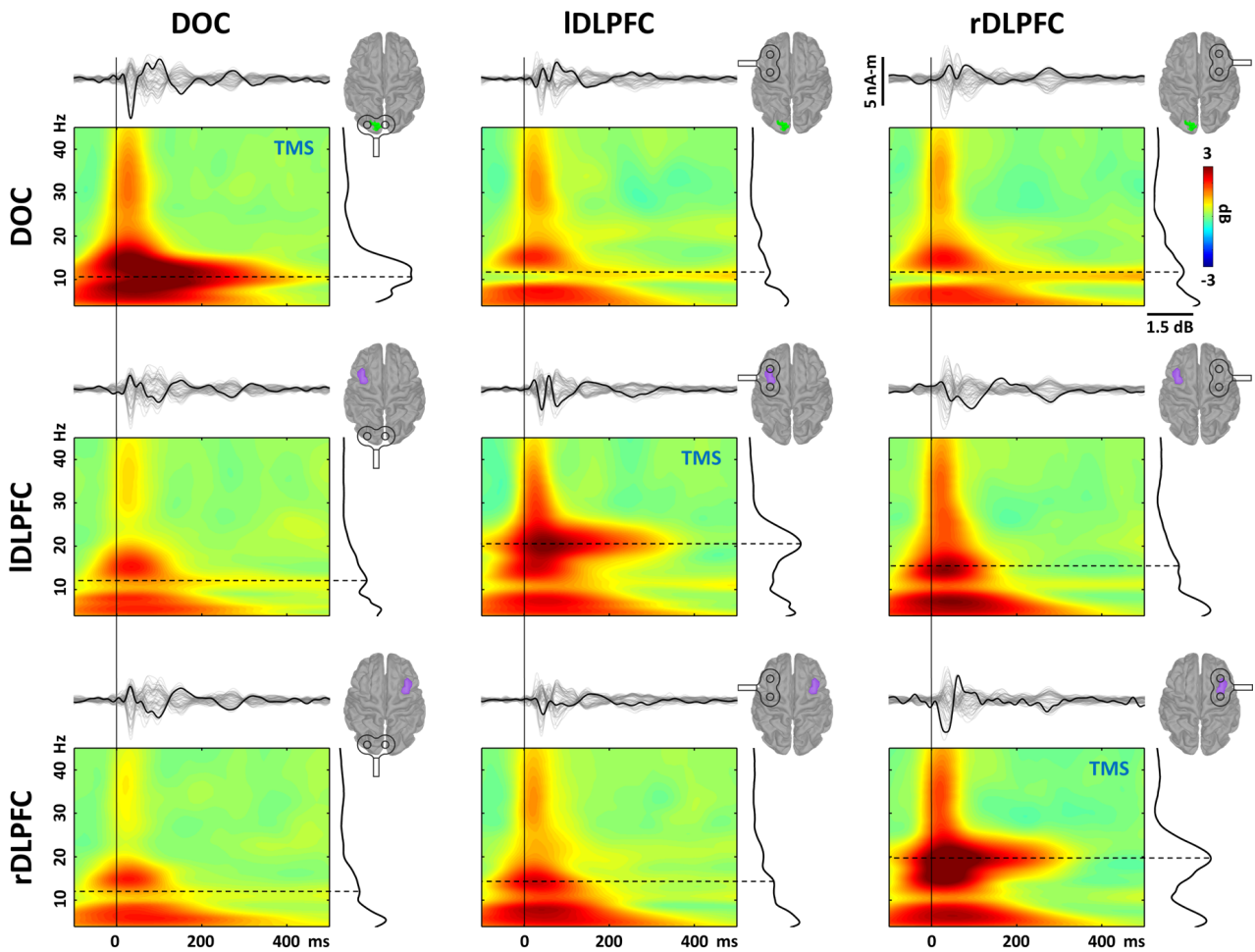


Figure 4. Average source-based Event-Related Spectral Perturbations (ERSP). The time-frequency plots show the average TMS-related ERSPs extracted from three different ROIs (DOC, IDLPFC, rDLPFC, in rows) as a function of the three corresponding TMS blocks (in columns). The time-frequency plots on the diagonal line marked by the TMS label show the ERSP for the specific ROI targeted in each TMS block. The trace plots above each time-frequency plot represent butterfly plots of all TMS-evoked potentials, where the black trace highlights the ROI used in the analysis. The black line plotted at the right of each time-frequency plot depicts the power spectrum profile elicited during the first 400 ms after TMS. The black dashed lines highlight the frequency corresponding to the natural frequency. DOC, dorsal occipital cortex; IDLPFC, left dorsolateral prefrontal cortex; rDLPFC, right dorsolateral prefrontal cortex.

3.2 Site-specific TMS modulation of ERSP responses

As shown in the left panel of Figure 5A, the TFCE analysis revealed that TMS of the DOC significantly modulated the ERSPs recorded from the target channel PO3, with a significant early, broadband increase in power that was stronger and more sustained for alpha-band frequencies (peak effect: 9.25 Hz, 170 ms; $t(11) = 19.39, p < .001, d = 5.60$). The increase in PO3 power was

significantly larger after TMS of the DOC as compared to TMS of both IDLPFC and rDLPFC in a cluster extending approximately from -100 to 370 ms and involving the frequencies between 7 and 15 Hz (DOC vs. IDLPFC peak effect: 9.75 Hz, 180 ms; $t(11) = 12.91, p < .001, d = 3.73$. DOC vs. rDLPFC peak effect: 9.5 Hz, 130 ms; $t(11) = 13.17, p < .001, d = 3.80$. Figure 5A).

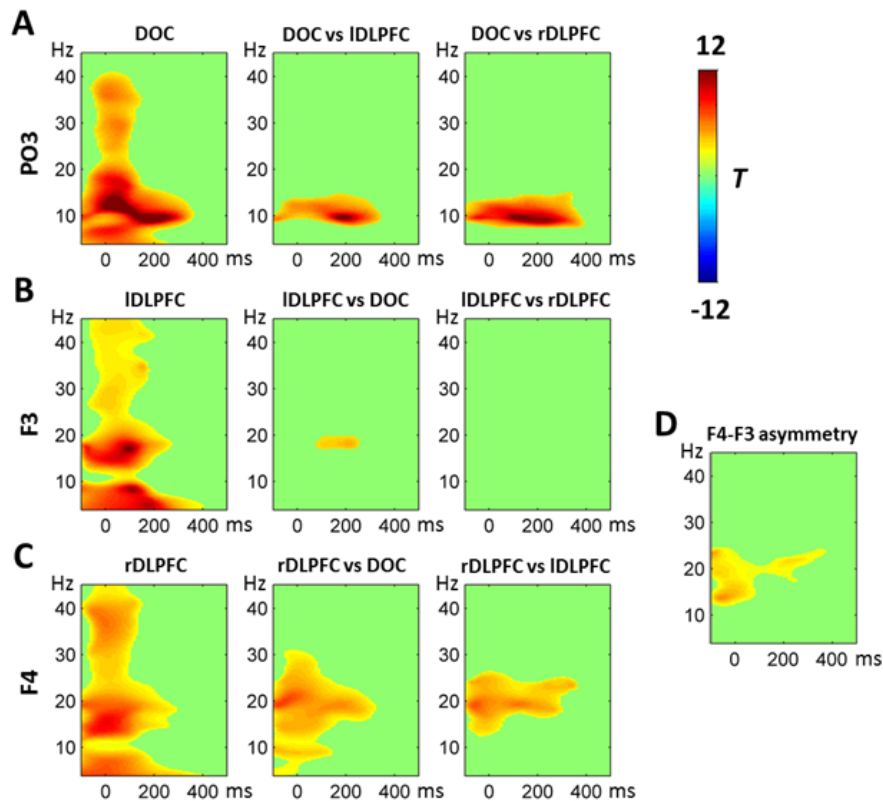


Figure 5. Threshold Free Cluster Enhancement results, scalp-based analysis. The time-frequency plots show the results of the Threshold Free Cluster Enhancement (TFCE) analysis. Only significant t-values ($p < .05$) are shown in a color scale. Rows A, B and C depict TFCE results on PO3, F3 and F4 channels, respectively, for the TMS block targeting each channel and the contrasts between that block and the two other blocks (columns from left to right). Panel D shows TFCE results for the comparison assessing prefrontal asymmetries in the TMS effect, that is, the contrast between the difference in F4 ERSP between rDLPFC and IDLPFC TMS blocks and the difference in F3 ERSP between IDLPFC and rDLPFC TMS blocks. DOC, dorsal occipital cortex block; IDLPFC, left dorsolateral prefrontal cortex block; rDLPFC, right dorsolateral prefrontal cortex block.

Moreover, the TMS of the IDLPFC modulated the ERSPs recorded from the target channel F3, with a significant early, broadband increase in power that was stronger and more sustained for theta- and beta-band frequencies (peak effect: 17 Hz, 100 ms; $t(11) = 12.05, p < .001, d = 3.48$; see

left panel of Figure 5B). The power increase in F3 was significantly larger after TMS of the IDLPFC as compared to TMS of the DOC in a cluster extending approximately from 100 to 250 ms and involving beta frequencies between 17 and 20 Hz (peak effect: 18.25 Hz, 210 ms; $t(11) = 4.67$, $p < .001$, $d = 1.35$). However, no significant differences were observed when contrasting the ERSPs computed for the F3 channel between the TMS of the left and right DLPFC (Figure 5B).

Finally, the TMS of the rDLPFC significantly modulated the ERSPs recorded from the target channel F4, with a significant early, broadband increase in power that was more sustained for theta- and beta-band frequencies (peak effect: 15.5 Hz, 10 ms; $t(11) = 9.09$, $p < .001$, $d = 2.62$; see left panel of Figure 5C). The increase in F4 power was significantly larger after TMS of the rDLPFC as compared to TMS of the DOC in a cluster extending from -100 to 320 ms and involving all the frequencies up to 30 Hz, although the differences were more evident for the beta frequencies between 16 and 22 Hz (peak effect: 19.25 Hz, 170 ms; $t(11) = 5.53$, $p < .001$, $d = 1.60$). Moreover, significant differences were also observed when contrasting the ERSPs computed for the F4 channel between the TMS of the right and left DLPFC, with a significant cluster extending from -100 to 360 ms and involving the beta frequencies between 16 and 25 Hz (peak effect: 19.25 Hz, 120 ms; $t(11) = 6.05$, $p < .001$, $d = 1.75$; Figure 5C).

More importantly, an additional analysis revealed a hemispheric asymmetry in the effect of TMS on prefrontal oscillations. Indeed, the TMS-related increase in rDLPFC beta power (i.e., the difference in F4 ERSP between rDLPFC and IDLPFC) was significantly greater than the TMS-related increase in IDLPFC beta power (i.e., the difference in F3 ERSP between IDLPFC and rDLPFC) in a cluster involving beta frequencies (12-24 Hz) between -100 and 80 ms and extending up to 360 ms for frequencies between 18 and 24 Hz (peak effect: 21.75 Hz, 230 ms; $t(11) = 3.86$, $p < .003$, $d = 1.11$; Figure 5D). A similar result was observed when contrasting directly the F4 ERSP in the rDLPFC stimulation with the F3 ERSP in the IDLPFC stimulation, with a cluster involving beta frequencies (12-24 Hz) between -100 and 80 ms.

As shown in Figure 6, source-based analyses generally confirmed the results observed in the scalp-based ones. The source-based TFCE analysis revealed that TMS of the DOC significantly modulated the ERSPs recorded from the target ROI, with a significant early, broadband increase in power that was stronger and more sustained for alpha-band frequencies (peak effect: 9.25 Hz, 110 ms; $t(11) = 18.17, p < .001, d = 5.25$; see left panel of Figure 6A). The increase in DOC power was significantly larger after DOC block as compared to both IDLPFC and rDLPFC blocks in a cluster extending approximately from -100 to 400 ms and involving mainly the frequencies between 8 and 15 Hz (DOC vs IDLPFC peak effect: 9.5 Hz, 50 ms; $t(11) = 10.38, p < .001, d = 3.00$. DOC vs rDLPFC peak effect: 9.5 Hz, 100 ms; $t(11) = 13.19, p < .001, d = 3.81$. Figure 6A).

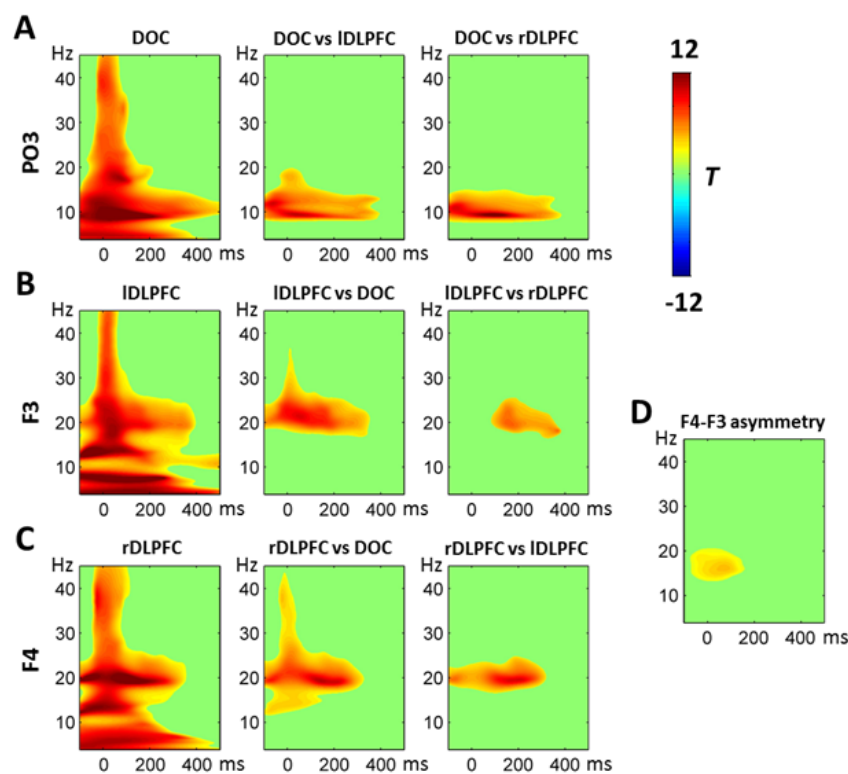


Figure 6. Threshold Free Cluster Enhancement results, source-based analysis. The time-frequency plots show the results of the Threshold Free Cluster Enhancement (TFCE) analysis performed on the ERSPs computed on the cortical ROIs. Rows A, B and C depict TFCE results on DOC, IDLPFC, and rDLPFC ROIs, respectively, for the TMS block targeting each ROI and the contrasts between that block and the two other blocks (columns from left to right). Panel D shows TFCE results for the contrast assessing prefrontal asymmetries in the TMS effect, that is, the contrast between the difference in the ERSP for the rDLPFC ROI between rDLPFC and IDLPFC TMS blocks and the difference in the ERSP for the IDLPFC ROI between IDLPFC and rDLPFC TMS blocks. Conventions are as in Figure 5.

Moreover, the TMS of the IDLPFC modulated the ERSPs recorded from the target ROI, with a significant early, broadband increase in power that was stronger and more sustained for theta-, alpha-, and beta-band frequencies (peak effect: 7.5 Hz, 230 ms; $t(11) = 9.55, p < .001, d = 2.76$; see left panel of Figure 6B). The power increase in IDLPFC was significantly larger after the IDLPFC TMS block as compared to both the other blocks in a cluster extending up to approximately 400 ms and involving mainly beta frequencies between 17 and 25 Hz (IDLPFC vs. DOC peak effect: 21.5 Hz, 50 ms; $t(11) = 9.55, p < .001, d = 2.76$. IDLPFC vs. rDLPFC peak effect: 20 Hz, 160 ms; $t(11) = 6.58, p < .001, d = 1.90$. Figure 6B).

Finally, the TMS of the rDLPFC significantly modulated the ERSPs recorded from the target ROI, with a significant early, broadband increase in power that was more sustained for theta- and beta-band frequencies (peak effect: 19.75 Hz, 110 ms; $t(11) = 15.10, p < .001, d = 4.36$; see left panel of Figure 6C). The increase in rDLPFC power was significantly larger after the rDLPFC TMS block as compared to both the other blocks in a cluster extending approximately from -100 to 300 ms and involving mainly the beta frequencies between 16 and 24 Hz (rDLPFC vs. DOC peak effect: 19.5 Hz, 140 ms; $t(11) = 10.53, p < .001, d = 3.04$. rDLPFC vs. IDLPFC peak effect: 19.5 Hz, 200 ms; $t(11) = 19.6, p < .001, d = 5.66$. Figure 6C).

A further TFCE analysis was performed to specifically test for hemispheric asymmetries in the effect of TMS on prefrontal activity. This analysis contrasted the specific TMS-related power increase for rDLPFC (i.e., the difference in the ERSP for the rDLPFC ROI between rDLPFC and IDLPFC blocks) and IDLPFC (i.e., the difference in the ERSP for the IDLPFC ROI between IDLPFC and rDLPFC blocks). The results showed that the specific TMS-related power increase was greater for rDLPFC than IDLPFC in a cluster extending from -70 to 150 ms and involving beta frequencies between 13 and 20 Hz (peak effect: 16.25 Hz, 80 ms; $t(11) = 4.34, p < .002, d = 1.25$, Figure 6D). A similar result was observed when contrasting directly the ERSP for the rDLPFC ROI

in the rDLPFC block with the ERSP for the IDLPFC ROI in the IDLPFC block, with a cluster involving beta frequencies (13-21 Hz) between -90 and 170 ms.

3.3 Natural frequencies

Figure 7A shows the average power spectrum profiles elicited by the TMS of DOC, IDLPFC, and rDLPFC over the respective target channels. The TFCE-corrected paired-sample t-tests revealed that the spectral profile elicited by the TMS of DOC, as compared to those elicited by TMS of both IDLPFC and rDLPFC, had significantly greater power in the 7.25-14.25 Hz frequency range (DOC vs. IDLPFC peak effect: 9.25 Hz; $t(11) = 7.67, p < .001, d = 2.21$. DOC vs. rDLPFC peak effect: 9.25 Hz; $t(11) = 5.31, p < .001, d = 1.53$. Figure 7A), as well as significantly lower power in the 16.5-24.5 Hz frequency range (DOC vs. IDLPFC peak effect: 17.5 Hz; $t(11) = 8.02, p < .001, d = 2.31$. DOC vs. rDLPFC peak effect: 18.5 Hz; $t(11) = 4.11, p < .002, d = 1.19$. Figure 7A). Conversely, the spectral profiles elicited by the TMS of IDLPFC and rDLPFC did not significantly differ between each other (peak effect: 20.25 Hz; $t(11) = 1.65, p < .126, d = 0.48$). Across participants, the natural frequency of the local scalp response to stimulation of DOC, IDLPFC, and rDLPFC was, respectively, 10.58 Hz (SD = 2.5 Hz, range = 7.5-14 Hz), 18.77 Hz (SD = 3.1 Hz, range = 16-25 Hz), and 18.50 Hz (SD = 2.3 Hz, range = 15.5-21.75 Hz; see Figure 7A and Table S1 in Supplementary Material).

Similar results were observed for the source-based analysis of natural frequencies, as shown in Figure 7B. The TFCE-corrected paired-sample t-tests revealed that the spectral profile elicited by the TMS of DOC, as compared to those elicited by TMS of both IDLPFC and rDLPFC, had significantly greater power in the frequency range between 7.5 and 14.5 Hz (DOC vs. IDLPFC peak effect: 8.75 Hz, $t(11) = 6.17, p < .001, d = 1.78$; DOC vs. rDLPFC peak effect: 9 Hz, $t(11) = 8.39, p < .001, d = 2.42$. Figure 7B), as well as significantly lower power in the frequency range approximately between 17 and 26 Hz (DOC vs. IDLPFC peak effect: 19.75 Hz, $t(11) = 5.92, p <$

.001, $d = 1.71$; DOC vs. rDLPFC peak effect: 19.25 Hz, $t(11) = 10.55$, $p < .001$, $d = 3.05$. Figure 7B). Again, the spectral profiles elicited by the TMS of IDLPFC and rDLPFC did not significantly differ between each other (peak effect: 18.25 Hz, $t(11) = 1.20$, $p = .257$, $d = 0.35$). Across all participants, the natural frequency of the local scalp response to stimulation of DOC, IDLPFC, and rDLPFC was, respectively, 10.87 Hz (SD = 2.14 Hz, range = 7.7-14 Hz), 20.3 Hz (SD = 1.86 Hz, range = 17-22.7 Hz), and 19.6 Hz (SD = 1.83 Hz, range = 17-21.8 Hz) (see Figure 7B and Table S1 in Supplementary Material).

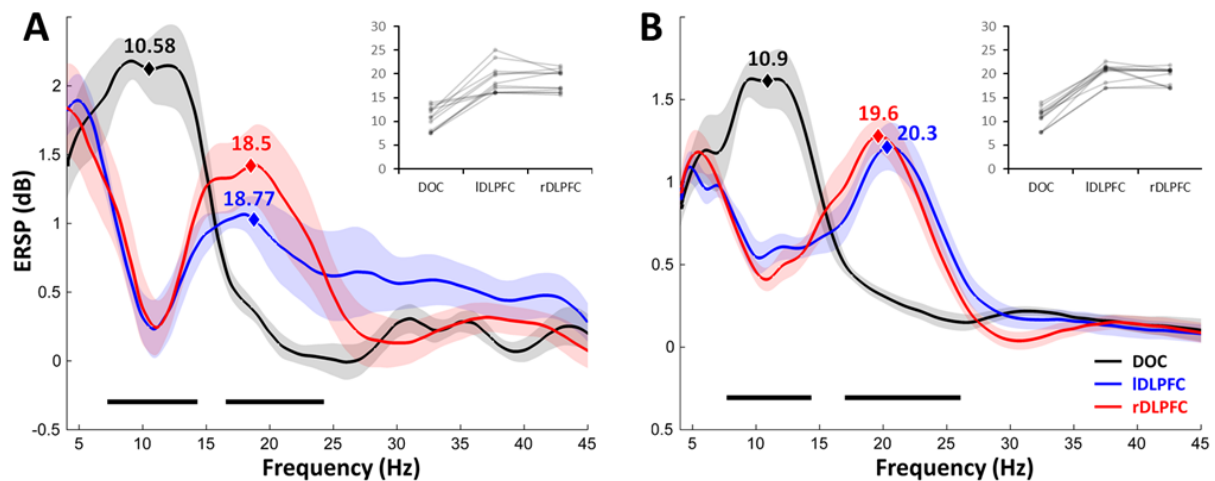


Figure 7. Natural frequencies. The plots show the average power spectrum profiles elicited by the TMS of DOC, IDLPFC, and rDLPFC during the first 400 ms post-TMS over the respective target channels (A) and cortical ROIs (B). The shaded regions represent the standard error of the mean. The black lines below the power spectrum profiles indicate the frequencies with significant differences between DOC and the other two TMS blocks (paired-sample t-tests corrected for multiple comparisons across-frequencies with the TFCE approach). The mean natural frequencies (Hz) are indicated by diamond markers. The insets show the natural frequencies for each participant in the three TMS blocks.

4. Discussion

We used sp-TMS to perturb in a controlled manner corticothalamic circuits and investigate whether we could extend previous findings showing that these circuits become tuned to specific natural frequencies upon TMS pulse (Canali et al., 2017, 2015; Ferrarelli et al., 2012; Rosanova et al., 2009). In particular, we investigated for the first time possible inter-hemispheric differences in TMS-related natural oscillations in two homologous prefrontal regions.

A first result was that, independently of the stimulation site, TMS clearly produced a widespread increase in theta power, compatibly with the predominant theta-band activity already observed with resting-state electrocorticography over several cortical sites (Groppe et al., 2013). However, this increase in theta power was unspecific, as revealed by our cross-site analysis, and thus would not reflect the dominant frequency of oscillation of the intrinsic activity of the regions we stimulated (Ozdemir et al., 2020). These unspecific theta activations could be due, at least in part, to the indirect multisensory (i.e., auditory and somatosensory) responses to TMS (Conde et al., 2019); this is particularly true for the AEP, as the N1-P2 complex is the main waveform contributing to the TMS-induced oscillations in the theta band (Van Der Werf & Paus, 2006). We used earplugs instead of active noise masking and, thus, TMS noise was only partially masked. A somatosensory stimulation as well as a bone conduction contribution may not be excluded. As we already noted, however, our analytical approach allowed us to control for these potential unspecific effects, especially those evoked by the TMS click, since they can be assumed to be virtually the same across TMS blocks (see footnote 2). In line with this interpretation, the N1 and P2 components of the AEP did not significantly differ across TMS sites. Previous works adopting a similar approach as ours did not investigate theta frequencies, as they only reported frequencies >8 Hz (Ferrarelli et al., 2012; Rosanova et al., 2009; Stanfield and Wiener, 2019), preventing a comparison of results. Future studies should further investigate the TMS effect on theta band to clarify both its functional role and contribution to natural frequencies and how and to what degree it is impacted by auditory (and somatosensory) responses to TMS.

We also observed that each region tended to resonate at approximately its own characteristic frequency when TMS was directly applied (Figures 2 and 4). Since we were also interested in assessing the specificity of the natural frequency in each stimulation site, we statistically compared, for the first time, the TMS effect for each recording channel across TMS sites. Importantly, the TMS-related ERSP showed magnitude and frequency profiles that were specific for the stimulated

site, as they were characterized by higher frequencies in lateral prefrontal cortices as compared to the occipital cortex. In particular, there was a significantly larger increase in prefrontal beta power when TMS was applied over each DLPFC than over the DOC and there was a significantly larger increase in alpha power when the TMS was applied over the DOC than the DLPFCs (Figures 5 and 6).

Our results showed that the TMS of the three cortical sites resulted, during the first 400 ms, in significantly different power spectrum profiles with specific natural frequencies (Figure 7). In particular, TMS over the occipital site resulted in a spectral profile characterized by a peak in the alpha band and a natural frequency of 10.58 Hz, in line with previous findings (Ferrarelli et al., 2012; Rosanova et al., 2009; but see Stanfield and Wiener, 2019), while TMS over the left and right DLPFC resulted in similar spectral profiles characterized by a peak in the beta band and a natural frequency of 18.77 and 18.5 Hz, respectively, compatible with previous findings (Ambrosini et al., 2020; Ambrosini and Vallesi, 2017, 2016; Groppe et al., 2013; Tafuro et al., 2019). These results seem however at odds with those reported by Ferrarelli et al. (2012) who found TMS-induced beta-gamma prefrontal activity, with a 31 Hz natural frequency. This discrepancy may be due to the methodological differences between these studies and to the limitations of our study, as reported below. Notably, however, their stimulated region was more medial and rostral (MNI:-15, 55, 38) than our mid-DLPFC spot (MNI: -34, 14, 54), which could contribute to explain the discrepancy.

Another goal of this study was to investigate the existence of hemispheric lateralization of natural frequencies for homologous stimulation sites. The TMS-related specific increase in beta activity was weaker for the left than right DLPFC (see Figure 5D and 6D). Indeed, the beta power increase in IDLPFC was more similar when it was stimulated either directly or indirectly. Conversely, the stronger TMS-related specific increase in rDLPFC beta activity suggests that this region is more specifically tuned to the natural beta frequency when it is directly stimulated by TMS than when the left counterpart (or a posterior region) is stimulated. It would be important in

future studies to understand whether these hemispheric asymmetries are more related to the dominance status of the two homologous regions or are a more general feature.

In the present study we did not restrict recruitment to right-handed individuals. While this could be admittedly seen as a limitation, it is also true that hand-preference could not be considered a reliable general proxy of hemispheric dominance outside the motor domain (Knecht et al., 2000; Pujol et al., 1999). Nonetheless, it is reassuring that our main results did not change after excluding non-right-handed participants (see Supplementary Material, Figures S9-11).

Moreover, the scalp-based results were confirmed on the targeted cortical regions as reconstructed with source analysis. Our results suggest that we successfully targeted the intended cortical regions and that our scalp-based analytical approach succeeded in isolating specific TMS-related ERSP modulations. Nonetheless, these results should be taken with caution. The absence of a neuronavigation procedure to precisely identify TMS target cortical regions and the fact that we did not use individual anatomies in performing the source reconstruction represent limitations of the present study, which did not allow us to ensure the accuracy of the stimulation at the single subject level. Further, unlike Rosanova and colleagues (2011), we employed a fixed stimulation intensity corresponding to the individual rMT. However, as we already noted (see section 2.2), it is unlikely that this methodological difference could have affected our results.

Lastly, as we already noted, although TMS noise was attenuated by the use of earplugs, no further noise-masking procedure was adopted (e.g., Rosanova et al., 2011). Our control analyses on N1 and P2 components of the AEP showed that they did not significantly differ across the three stimulation sites. It is thus unlikely that this limitation of our study could have biased our statistical comparisons.

5. Conclusions

In conclusion, our findings show that the rDLPFC is more specifically tuned to its natural beta frequency when it is directly stimulated by TMS than when other regions are stimulated, while the IDLPFC shows a weaker TMS-related specific increase in beta activity, namely, a more similar beta increase both when it is stimulated directly and indirectly through right homologous stimulation. These results may inform future investigation on inter-hemispheric prefrontal interactions and clinical applications.

6. References

- Ambrosini, E., Capizzi, M., Arbula, S., Vallesi, A., 2020. Right-lateralized intrinsic brain dynamics predict monitoring abilities. *Cogn Affect Behav Neurosci* 20, 294–308. <https://doi.org/10.3758/s13415-020-00769-6>
- Ambrosini, E., Vallesi, A., 2017. Domain-general Stroop Performance and Hemispheric Asymmetries: A Resting-state EEG Study. *J Cogn Neurosci* 29, 769–779. https://doi.org/10.1162/jocn_a_01076
- Ambrosini, E., Vallesi, A., 2016. Asymmetry in prefrontal resting-state EEG spectral power underlies individual differences in phasic and sustained cognitive control. *Neuroimage* 124, 843–857. <https://doi.org/10.1016/j.neuroimage.2015.09.035>
- Artoni, F., Delorme, A., & Makeig, S. (2018). Applying dimension reduction to EEG data by Principal Component Analysis reduces the quality of its subsequent Independent Component decomposition. *NeuroImage* 175, 176–187.
- Baillet, S., Riera, J.J., Marin, G., Mangin, J.F., Aubert, J., Garnero, L., (2000). Evaluation of inverse methods and head models for EEG source localization using a human skull phantom. *Phys Med Biol* 46, 77–96. <https://doi.org/10.1088/0031-9155/46/1/306>
- Beam, W., Borckardt, J.J., Reeves, S.T., George, M.S., 2009. An efficient and accurate new method for locating the F3 position for prefrontal TMS applications. *Brain Stimul* 2, 50–54. <https://doi.org/10.1016/j.brs.2008.09.006>
- Bortoletto, M., Veniero, D., Thut, G., Miniussi, C., 2015. The contribution of TMS–EEG coregistration in the exploration of the human cortical connectome. *Neuroscience & Biobehavioral Reviews* 49, 114–124. <https://doi.org/10.1016/j.neubiorev.2014.12.014>
- Canali, P., Casarotto, S., Rosanova, M., Sferrazza-Papa, G., Casali, A.G., Gosseries, O., Massimini, M., Smeraldi, E., Colombo, C., Benedetti, F., 2017. Abnormal brain oscillations persist after recovery from bipolar depression. *Eur Psychiatry* 41, 10–15. <https://doi.org/10.1016/j.eurpsy.2016.10.005>
- Canali, P., Sarasso, S., Rosanova, M., Casarotto, S., Sferrazza-Papa, G., Gosseries, O., Fecchio, M., Massimini, M., Mariotti, M., Cavallaro, R., Smeraldi, E., Colombo, C., Benedetti, F., 2015. Shared reduction of oscillatory natural frequencies in bipolar disorder, major depressive disorder and schizophrenia. *J Affect Disord* 184, 111–115. <https://doi.org/10.1016/j.jad.2015.05.043>

- Cona, F., Zavaglia, M., Massimini, M., Rosanova, M., Ursino, M., 2011. A neural mass model of interconnected regions simulates rhythm propagation observed via TMS-EEG. *Neuroimage* 57, 1045–1058. <https://doi.org/10.1016/j.neuroimage.2011.05.007>
- Conde, V., Tomasevic, L., Akopian, I., Stanek, K., Saturnino, G. B., Thielscher, A., ... & Siebner, H. R. (2019). The non-transcranial TMS-evoked potential is an inherent source of ambiguity in TMS-EEG studies. *Neuroimage*, 185, 300-312.
- Delorme, A., Palmer, J., Onton, J., Oostenveld, R., & Makeig, S. (2012). Independent EEG sources are dipolar. *PloS one*, 7(2), e30135.
- Delorme, A., & Makeig, S. (2004). EEGLAB: an open source toolbox for analysis of single-trial EEG dynamics including independent component analysis. *Journal of Neuroscience Methods*, 134(1), 9-21.
- Destrieux, C., Fischl, B., Dale, A., Halgren, E., 2010. Automatic parcellation of human cortical gyri and sulci using standard anatomical nomenclature. *NeuroImage* 53, 1-15. <https://doi.org/10.1016/j.neuroimage.2010.06.010>.
- Faul, F., Erdfelder, E., Buchner, A., Lang, A.-G., 2009. Statistical power analyses using G*Power 3.1: Tests for correlation and regression analyses. *Behavior Research Methods* 41, 1149–1160. <https://doi.org/10.3758/BRM.41.4.1149>
- Feige, B., Scheffler, K., Esposito, F., Di Salle, F., Hennig, J., Seifritz, E., 2005. Cortical and subcortical correlates of electroencephalographic alpha rhythm modulation. *J Neurophysiol* 93, 2864–2872. <https://doi.org/10.1152/jn.00721.2004>
- Ferrarelli, F., Sarasso, S., Guller, Y., Riedner, B.A., Peterson, M.J., Bellesi, M., Massimini, M., Postle, B.R., Tononi, G., 2012. Reduced natural oscillatory frequency of frontal thalamocortical circuits in schizophrenia. *Arch. Gen. Psychiatry* 69, 766–774. <https://doi.org/10.1001/archgenpsychiatry.2012.147>
- Finisguerra, A., Borgatti, R., Urgesi, C., 2019. Non-invasive Brain Stimulation for the Rehabilitation of Children and Adolescents With Neurodevelopmental Disorders: A Systematic Review. *Front Psychol* 10, 135. <https://doi.org/10.3389/fpsyg.2019.00135>
- Fischl, B., Sereno, M.I., Tootell, R.B.H., Dale, A.M., 1999. High-resolution intersubject averaging and a coordinate system for the cortical surface. *Human Brain Mapping* 8, 272–84. [https://doi.org/10.1002/\(SICI\)1097-0193\(1999\)8:4<272::AID-HBM10>3.0.CO;2-4](https://doi.org/10.1002/(SICI)1097-0193(1999)8:4<272::AID-HBM10>3.0.CO;2-4).
- Fitzgerald, P.B., Daskalakis, Z.J., 2012. A practical guide to the use of repetitive transcranial magnetic stimulation in the treatment of depression. *Brain Stimul* 5, 287–296. <https://doi.org/10.1016/j.brs.2011.03.006>
- Fitzgerald, P.B., Maller, J.J., Hoy, K.E., Thomson, R., Daskalakis, Z.J., 2009. Exploring the optimal site for the localization of dorsolateral prefrontal cortex in brain stimulation experiments. *Brain Stimul* 2, 234–237. <https://doi.org/10.1016/j.brs.2009.03.002>
- Fox, M.D., Liu, H., Pascual-Leone, A., 2013. Identification of reproducible individualized targets for treatment of depression with TMS based on intrinsic connectivity. *Neuroimage* 66, 151–160. <https://doi.org/10.1016/j.neuroimage.2012.10.082>
- Fries, P., 2005. A mechanism for cognitive dynamics: neuronal communication through neuronal coherence. *Trends in Cognitive Sciences* 9, 474–480. <https://doi.org/10.1016/j.tics.2005.08.011>
- Gabard-Durnam, L. J., Mendez Leal, A. S., Wilkinson, C. L., & Levin, A. R. (2018). The Harvard Automated Processing Pipeline for Electroencephalography (HAPPE): standardized processing software for developmental and high-artifact data. *Frontiers in Neuroscience*, 12, 97.
- Gramfort, A., Papadopoulos, T., Olivi, E., Clerc, M., (2010). OpenMEEG: opensource software for quasistatic bioelectromagnetics. *BioMedical Engineering OnLine* 9, 45. <https://doi.org/10.1186/1475-925X-9-45>.

- Grandchamp, R., Delorme, A., 2011. Single-Trial Normalization for Event-Related Spectral Decomposition Reduces Sensitivity to Noisy Trials. *Front Psychol* 2, 236. <https://doi.org/10.3389/fpsyg.2011.00236>
- Groppe, D.M., Bickel, S., Keller, C.J., Jain, S.K., Hwang, S.T., Harden, C., Mehta, A.D., 2013. Dominant frequencies of resting human brain activity as measured by the electrocorticogram. *Neuroimage* 79, 223–233. <https://doi.org/10.1016/j.neuroimage.2013.04.044>
- Habib, R., Nyberg, L., Tulving, E., 2003. Hemispheric asymmetries of memory: the HERA model revisited. *Trends Cogn Sci* 7, 241–245. [https://doi.org/10.1016/s1364-6613\(03\)00110-4](https://doi.org/10.1016/s1364-6613(03)00110-4)
- Herwig, U., Satrapi, P., Schönfeldt-Lecuona, C., 2003. Using the international 10-20 EEG system for positioning of transcranial magnetic stimulation. *Brain Topogr* 16, 95–99. <https://doi.org/10.1023/b:brat.0000006333.93597.9d>
- Hone-Blanchet, A., Ciraulo, D.A., Pascual-Leone, A., Fecteau, S., 2015. Noninvasive brain stimulation to suppress craving in substance use disorders: review of human evidence and methodological considerations for future work. *Neurosci Biobehav Rev* 59, 184–200. <https://doi.org/10.1016/j.neubiorev.2015.10.001>
- Knecht, S., Dräger, B., Deppe, M., Bobe, L., Lohmann, H., Flöel, A., Ringelstein, E.B., Henningsen, H., 2000. Handedness and hemispheric language dominance in healthy humans. *Brain* 123(12), 2512–2518. <https://doi.org/10.1093/brain/123.12.2512>
- Laufs, H., Kleinschmidt, A., Beyerle, A., Eger, E., Salek-Haddadi, A., Preibisch, C., Krakow, K., 2003. EEG-correlated fMRI of human alpha activity. *Neuroimage* 19, 1463–1476. [https://doi.org/10.1016/s1053-8119\(03\)00286-6](https://doi.org/10.1016/s1053-8119(03)00286-6)
- Manganotti, P., Formaggio, E., Del Felice, A., Storti, S. F., Zamboni, A., Bertoldo, A., ... & Toffolo, G. M. (2013). Time-frequency analysis of short-lasting modulation of EEG induced by TMS during wake, sleep deprivation and sleep. *Frontiers in Human Neuroscience* 7, 767.
- Mantini, D., Perrucci, M.G., Del Gratta, C., Romani, G.L., Corbetta, M., 2007. Electrophysiological signatures of resting state networks in the human brain. *Proc. Natl. Acad. Sci. U.S.A.* 104, 13170–13175. <https://doi.org/10.1073/pnas.0700668104>
- Moosmann, M., Ritter, P., Krastel, I., Brink, A., Thees, S., Blankenburg, F., Taskin, B., Obrig, H., Villringer, A., 2003. Correlates of alpha rhythm in functional magnetic resonance imaging and near infrared spectroscopy. *Neuroimage* 20, 145–158. [https://doi.org/10.1016/s1053-8119\(03\)00344-6](https://doi.org/10.1016/s1053-8119(03)00344-6)
- Nee, D.E., D’Esposito, M., 2017. Causal evidence for lateral prefrontal cortex dynamics supporting cognitive control. *Elife* 6, e28040. <https://doi.org/10.7554/eLife.28040>
- Nolan, H., Whelan, R., & Reilly, R. B. (2010). FASTER: fully automated statistical thresholding for EEG artifact rejection. *Journal of Neuroscience Methods* 192(1), 152–162.
- Oldfield, R.C., 1971. The assessment and analysis of handedness: the Edinburgh inventory. *Neuropsychologia* 9, 97–113.
- Ozdemir, R.A., Tadayon, E., Boucher, P., Momi, D., Karakhanyan, K.A., Fox, M.D., Halko, M.A., Pascual-Leone, A., Shafi, M.M., Santarnecchi, E., 2020. Individualized perturbation of the human connectome reveals reproducible biomarkers of network dynamics relevant to cognition. *Proc. Natl. Acad. Sci. U.S.A.* 117, 8115–8125. <https://doi.org/10.1073/pnas.1911240117>
- Perrin, F., Pernier, J., Bertrand, O., Echallier, J.F., 1989. Spherical splines for scalp potential and current density mapping. *Electroencephalogr Clin Neurophysiol* 72, 184–187. [https://doi.org/10.1016/0013-4694\(89\)90180-6](https://doi.org/10.1016/0013-4694(89)90180-6)
- Pujol, J., Deus, J., Losilla, J.M., Capdevila, A., 1999. Cerebral lateralization of language in normal left-handed people studied by functional MRI. *Neurology* 52, 1038–1043. <https://doi.org/10.1212/wnl.52.5.1038>

- Rogasch, N.C., Sullivan, C., Thomson, R.H., Rose, N.S., Bailey, N.W., Fitzgerald, P.B., Farzan, F., Hernandez-Pavon, J.C., 2017. Analysing concurrent transcranial magnetic stimulation and electroencephalographic data: A review and introduction to the open-source TESA software. *Neuroimage* 147, 934–951. <https://doi.org/10.1016/j.neuroimage.2016.10.031>
- Rogasch, N. C., Thomson, R. H., Farzan, F., Fitzgibbon, B. M., Bailey, N. W., Hernandez-Pavon, J. C., ... & Fitzgerald, P. B. (2014). Removing artefacts from TMS-EEG recordings using independent component analysis: importance for assessing prefrontal and motor cortex network properties. *Neuroimage* 101, 425-439.
- Rosanova, M., Casali, A., Bellina, V., Resta, F., Mariotti, M., Massimini, M., 2009. Natural frequencies of human corticothalamic circuits. *J Neurosci* 29, 7679–7685. <https://doi.org/10.1523/JNEUROSCI.0445-09.2009>
- Rosanova, M., Casarotto, S., Pigorini, A., Canali, P., Casali, A.G., Massimini, M. (2011). Combining Transcranial Magnetic Stimulation with Electroencephalography to Study Human Cortical Excitability and Effective Connectivity. In: Fellin T., Halassa M. (eds) *Neuronal Network Analysis. Neuromethods, vol 67*. Humana Press. https://doi.org/10.1007/7657_2011_15
- Rossi, S., Hallett, M., Rossini, P.M., Pascual-Leone, A., 2009. Safety, ethical considerations, and application guidelines for the use of transcranial magnetic stimulation in clinical practice and research. *Clin Neurophysiol* 120, 2008–2039. <https://doi.org/10.1016/j.clinph.2009.08.016>
- Rossini, P.M., Barker, A.T., Berardelli, A., Caramia, M.D., Caruso, G., Cracco, R.Q., Dimitrijević, M.R., Hallett, M., Katayama, Y., Lücking, C.H., 1994. Non-invasive electrical and magnetic stimulation of the brain, spinal cord and roots: basic principles and procedures for routine clinical application. Report of an IFCN committee. *Electroencephalogr Clin Neurophysiol* 91, 79–92. [https://doi.org/10.1016/0013-4694\(94\)90029-9](https://doi.org/10.1016/0013-4694(94)90029-9)
- Smith, S.M., Nichols, T.E., 2009. Threshold-free cluster enhancement: addressing problems of smoothing, threshold dependence and localisation in cluster inference. *Neuroimage* 44, 83–98. <https://doi.org/10.1016/j.neuroimage.2008.03.061>
- Stanfield, C.T., Wiener, M., 2019. TMS-evoked oscillations in human cortical circuits: A search for natural frequencies. *bioRxiv* 614826. <https://doi.org/10.1101/614826>
- Stuss, D.T., Alexander, M.P., 2007. Is there a dysexecutive syndrome? *Philos. Trans. R. Soc. Lond., B, Biol. Sci.* 362, 901–915. <https://doi.org/10.1098/rstb.2007.2096>
- Tadel, F., Baillet, S., Mosher, J.C., Pantazis, D., Leahy, R.M., 2011. Brainstorm: A User-Friendly Application for MEG/EEG Analysis. *Computational Intelligence and Neuroscience*, e879716. <https://doi.org/10.1155/2011/879716>
- Tafuro, A., Ambrosini, E., Puccioni, O., Vallesi, A., 2019. Brain oscillations in cognitive control: A cross-sectional study with a spatial stroop task. *Neuropsychologia* 133, 107190. <https://doi.org/10.1016/j.neuropsychologia.2019.107190>
- Thielscher, A., Antunes, A., Saturnino, G.B., 2015. Field modeling for transcranial magnetic stimulation: A useful tool to understand the physiological effects of TMS? *Conf Proc IEEE Eng Med Biol Soc* 2015, 222–225. <https://doi.org/10.1109/EMBC.2015.7318340>
- Thut, G., Miniussi, C., Gross, J., 2012. The functional importance of rhythmic activity in the brain. *Curr. Biol.* 22, R658-663. <https://doi.org/10.1016/j.cub.2012.06.061>
- Thut, G., Veniero, D., Romei, V., Miniussi, C., Schyns, P., Gross, J., 2011. Rhythmic TMS causes local entrainment of natural oscillatory signatures. *Curr. Biol.* 21, 1176–1185. <https://doi.org/10.1016/j.cub.2011.05.049>
- Vallesi, A., 2012. Organisation of executive functions: Hemispheric asymmetries. *Journal of Cognitive Psychology* 24, 367–386. <https://doi.org/10.1080/20445911.2012.678992>

- Van Der Werf, Y. D., & Paus, T. (2006). The neural response to transcranial magnetic stimulation of the human motor cortex. I. Intracortical and cortico-cortical contributions. *Experimental Brain Research*, *175*(2), 231-245.
- Wassermann, E.M., 1998. Risk and safety of repetitive transcranial magnetic stimulation: report and suggested guidelines from the International Workshop on the Safety of Repetitive Transcranial Magnetic Stimulation, June 5-7, 1996. *Electroencephalogr Clin Neurophysiol* *108*, 1–16. [https://doi.org/10.1016/s0168-5597\(97\)00096-8](https://doi.org/10.1016/s0168-5597(97)00096-8)